Eur. Phys. J. D **2**, 45–52 (1998)

THE EUROPEAN PHYSICAL JOURNAL D

Cusp satellite bands in the spectrum of Cs_2 molecule

D. Veza[a], R. Beuc, S. Milošević, and G. Pichler

Institute of Physics, P.O. Box 304, 10000 Zagreb, Croatia

Received: 1 October 1997 / Revised: 14 January 1998 / Accepted: 24 February 1998

Abstract. We report measurements and a theoretical explanation of the cusp-shaped satellite bands in the blue wing of the cesium D_2 resonance line which have been observed for the first time. The bands are identified as $1\,^3\Pi_g(2_g, 1_g, 0_g^+, 0_g^-) \leftarrow a\,^3\Sigma_u^+(1_u, 0_u^+)$ transitions where the upper state dissociates into the $6\,^2P_{3/2}+6\,^2S_{1/2}$ atomic asymptote. The experiment has been performed using a standard absorption setup, computer controlled data acquisition and computer data processing. We have shown that the peculiar shape of the $1\,^3\Pi_g(0_g^+) - a\,^3\Sigma_u^+(1_u)$ difference-potential curve is solely responsible for the spectrum containing the cusp-shaped satellite bands. The appearance of these satellite bands has been discussed and explained relating the theory of satellite bands to the catastrophe theory. The shape of the line wing and of the satellite bands have been calculated using the Fourier transform technique. To ensure a more stringent comparison between the experimental and the theoretical spectrum, we have analyzed and compared the derivatives of the measured and the calculated satellite band shape. On the contrary to the customary direct comparison between the measured and the calculated absorption coefficient, the derivative clearly shows all differences and resemblances between satellite band profiles. The degree of coincidence of the experimentally observed and the theoretically calculated satellite band shape can be used as an ultimate check on the assessment of the quality of potential-energy curves involved in the formation of satellite bands.

PACS. 33.70.Jg Line and band widths, shapes, and shifts – 33.80.Gj Diffuse spectra; predissociation, photodissociation – 34.20.Cf Interatomic potentials and forces

1 Introduction

The visible and the near-infrared spectra of the cesium dimer have been extensively studied for many years by means of classical and laser spectroscopy. This is especially true for the bound-bound cesium dimer spectrum where several lowest singlet states of the Cs_2 molecule are known with high accuracy (3 (E) $^1\Sigma_u^+$ state [1], 2 (D) $^1\Sigma_u^+$ state [2,3], 2 (C) $^1\Pi_u$ state [4], 1 (B) $^1\Pi_u$ state [5], $1\,^1\Pi_g$ state [1], 1 (A) $^1\Sigma_u^+$ state [6], 1 (X) $^1\Sigma_g^+$ state [7], $2\,^1\Sigma_g^+$, and $3\,^1\Sigma_g^+$ states [8]). Because of the experimental difficulties in the investigations of the bound-free and free-free transitions, triplet states have less frequently been studied. However, in the case of transitions involving the lowest triplet states ($1\,^3\Sigma_g^+$, $1\,^3\Pi_g$, and $2\,^3\Pi_g$) and the 1 (a) $^3\Sigma_u^+$ ground state, two continuous features have been reported over the last two decades: a satellite band corresponding to the $1\,^3\Pi_g \leftarrow$1(a) $^3\Sigma_u^+$ transition [9–11] and a structured continuum corresponding to the $2\,^3\Pi_g \leftarrow$1(a) $^3\Sigma_u^+$ transition [12]. The $2\,^3\Pi_g \leftarrow$1(a) $^3\Sigma_u^+$ triplet-triplet transition has recently been studied under high resolution in a molecular beam [13–15].

The satellite bands in the far-blue wing of the cesium D_2 resonance line at 817, 827, and 835 nm were observed for the first time more than sixty years ago [16], but were discussed much later by Kusch and Hessel [17]. They interpreted these bands as resulting from predissociation to the repulsive states that dissociate to the $6\,^2P_{1/2;3/2} + 6\,^2S_{1/2}$ levels. Later research on the shape of the cesium first resonance lines opened up other possibilities for the explanation of these satellite bands. For example, in references [18–20] the quantitative explanation of the near-wing satellite bands and asymmetry of the alkali first resonance lines was based on the fact that the satellite bands are a consequence of the local extrema in the relevant potential-energy curves. Movre and Pichler [19,20] showed that the recoupling of angular momenta at large interatomic distances generates local extrema owing to the avoided crossings in the complex manifold of potential-energy curves emerging from the $^2S_{1/2} + {}^2P_{1/2}$ and $^2S_{1/2} + {}^2P_{3/2}$ asymptotic levels. According to the quasistatic theory of line shape [21], the local extrema in the relevant difference-potential curves are directly responsible for the appearance of satellite bands. The calculation of the line-wing shape based on this theory generates the singularity (*classical satellite* [22]) in the line wing at the position corresponding to the extremum in the difference potential curve. However, using the unified Franck-Condon (UFC) theory of the satellite band shape [23] and the known atomic interaction constants, the

[a] e-mail: veza@ifs.hr

position and the shape of the near-wing cesium satellite bands can be very accurately reproduced [24,25]. The spectral line satellites caused by the local extrema of the difference-potential curves are usually designated *rainbow satellite bands* [29], because of the analogy to the explanation and formation of rainbows [30].

The tentative origin of cesium and potassium far-wing satellite bands was discussed by Pichler *et al.* (Cs_2 case) [9] and by Beuc *et al.* (K_2 case) [26]. In the potassium case, it was shown that the interplay of the resonance, the van der Waals and the exchange interactions caused the appearance of the local maxima in the initially repulsive 2_g, 1_g, 0_g^- and 0_g^+ potential curves, resulting in the formation of the potassium far-wing triplet-satellite band at 721.4 nm and a shoulder at 748.5 nm. Thus, the spectroscopic identification and interpretation of satellite bands depend on a direct comparison between the experimental spectrum and the spectrum calculated from a chosen set of the potential-energy curves. Consequently, the calculation of the satellite band shape is a very sensitive test for the accuracy of the (usually *ab initio* calculated) potential-energy curves involved.

In spite of the large amount of work performed during the last two decades there still remains a lot to be done in Cs_2 spectroscopy, especially for the lowest triplet states. The achievement of the Bose-Einstein condensation (BEC), for example, depends critically on the ground-state scattering length [27,28]. In order to achieve a stable BEC in an assembly of atoms, the scattering length, characterizing the scattering of a pair of atoms at ultralow collision energies, must be positive and large. The magnitude and sign of the scattering length are extremely sensitive to details of the interatomic potentials involved in the collision event. The traditional procedure for the experimental determination of these potential-energy curves, or the procedure for testing the quality of the existing potential-energy curves is based on the comparison between the experiment and the shape of the line wing calculated within quasistatic theory. This procedure can supply data on the positions of local extrema, but not details of the difference-potential curve.

The purpose of this paper is to point out the existence of the *cusp satellite bands* using a more sensitive approach to the analysis and comparison of the measured and the calculated line-wing shape. Contrary to the *rainbow satellite bands* [29] caused by the local maximum in the difference-potential curve, the origin of the *cusp satellite bands* discussed here is different, and therefore should be distinguished from the rainbow satellites. The calculation of the line wing and the satellite shape has been performed using the Fourier transform technique and *ab initio* calculated cesium dimer potential-energy curves [31, 32]. The line wing and the satellite-shape analysis is based on a comparison of the *derivatives* of the measured and the calculated satellite band shape. We explain the origin and the shape of all satellite bands (the rainbow as well as the cusp-shaped) observed in the far-blue wing of the self-broadened cesium D_2 resonance line.

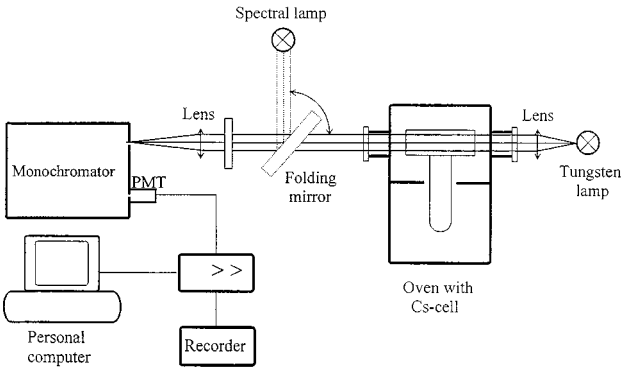

Fig. 1. The experimental setup for the measurements of the absorption coefficient.

This paper is organized as follows. Experimental details are described in Section 2. The observation and interpretation of the satellite bands are presented in Section 3. Section 4 contains the Fourier transform approach to the theoretical treatment of the atomic line shape. The role of the shape of the difference-potential curve for the determination of the shape of the corresponding satellite band is discussed in Section 5. Finally, conclusions are given in Section 6.

2 Experimental details

The experimental apparatus is shown in Figure 1. A T-shaped cell containing cesium liquid in the side arm was made of Pyrex glass. The cell was heated in a two-chamber oven having two independent heaters. The temperature of the bath (T_b, lower compartment) and the temperature of the cell (T_c, upper compartment) were measured by thermocouples and kept constant to ± 0.1 K during the measurement by active stabilization of the heating current. Note that the accurate stabilization and measurement of the bath temperature is of great importance because this temperature determines the vapor pressure and thus the atomic density in the upper part of the absorption cell. The atomic densities were calculated using the well-known relation for the vapor pressure-temperature curve [33]:

$$\log_{10} p = 11.0531 - \frac{4041}{T_b} - 1.35 \log_{10} T_b, \qquad (1)$$

where the pressure is given in Torr's and the temperature in degrees Kelvin. The atomic density (in m^{-3}) was determined from the ideal gas law:

$$N = 9.66 \times 10^{24} \frac{p}{T_c} \cdot \qquad (2)$$

We estimated the maximum variation of the cesium atom density in each run to be less than 1% of the nominal value. The accuracy in the determination of the nominal cesium pressure and atomic density is given by the accuracy of the measured vapor pressure-temperature curve and is about $\pm 15\%$ [33].

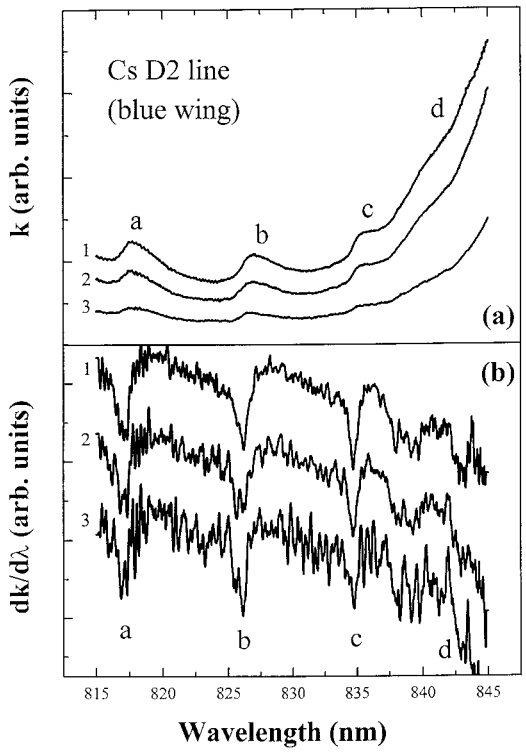

Fig. 2. The Cs D_2 line wing in the region from 815 nm to 845 nm for three temperature settings: $1 - T_c = 647$ K, $T_b = 625$ K, $N = (9.7 \pm 1.5) \times 10^{22}$ m^{-3}; $2 - T_c = 638$ K, $T_b = 615$ K, $N = (7.9 \pm 1.2) \times 10^{22}$ m^{-3}; $3 - T_c = 627$ K, $T_b = 595$ K, $N = (5.1 \pm 0.7) \times 10^{22}$ m^{-3}. (a) The absorption line-wing shapes for the three indicated temperature settings presented on a relative scale. (b) The corresponding first derivatives of the absorption line wing. The spectrum labeled "1" is used for further analysis.

The cell with the cesium vapor was irradiated by the continuous light from a halogen lamp. The light passing the absorption cell was analyzed using a monochromator with a resolution between 0.1 and 0.01 nm. The dispersed light was detected by a red-sensitive photomultiplier (EMI 9558QB). The signal was fed into a lock-in amplifier, digitized by an A/D converter and stored in a personal computer for further processing. The spectral range of interest, between 815 nm and 845 nm, was measured with a monochromator resolution of about 0.1 nm and a recording density of 200 points/nm. The absolute calibration of the wavelength scale, the monochromator resolution and the spectral dispersion were determined using a cesium low-pressure spectral lamp. The exact wavelength of all major spectral features ("a", "b", "c", but also each "d_i" - see also Fig. 3b), as well as their relative spectral position in each scan are reproducible within ± 2 points (± 0.01 nm). The far-blue wing of the cesium D_2 absorption line was measured at three different settings of the bath and the cell temperatures. Five independent subsequent scans were taken at each combination of the bath and the cell temperatures. Every absorption profile presented in Figure 2a (labeled 1, 2 or 3) is the average of these five scans, exactly overlapped resulting in an absorption profile with significantly reduced statistical noise.

Table 1. The assignment of the observed satellite bands in the far-blue wing of the Cs D_2 line. The classical satellite labeled c″ is not discernible in the experimental spectrum, most probably because of its position in the very strong resonance line wing.

Label	Transition	Location (nm)	Band origin
a	$2_g \leftarrow 1_u$	817	local maximum
b	$1_g \leftarrow 1_u, 0_u^-$	827	local maximum
c	$0_g^+ \leftarrow 1_u$	835	local maximum
d_2	$0_g^+ \leftarrow 1_u$	838	cusp satellite (type II)
c′	$0_g^+ \leftarrow 1_u$	842	local maximum
d_1	$0_g^+ \leftarrow 1_u$	843	cusp satellite (type I)
c″	$0_g^+ \leftarrow 1_u$	848	local minimum

3 Results

The observed satellite bands are assigned according to the discussion given by Pichler *et al.* [9]. In Table 1 we summarize the positions and the origin of all satellites observed in the blue wing of the cesium D_2 absorption line (λ_{centre}=852.1 nm). We note that in the blue wing of the cesium D_1 resonance line (λ_{centre}=894.4 nm) there exists one additional far-wing rainbow satellite at 875 nm [9]. The origin of this satellite band is similar to the origin of the rainbow-satellite bands of the D_2 absorption line and, for the sake of simplicity, will not be discussed here.

3.1 Observation

The line-wing shape was evaluated on the basis of the Beer-Lambert law and the results are presented in Figure 2a in the form of the reduced absorption coefficient. Since we were interested only in the *shape* of the reduced absorption coefficient in the region of satellite bands, and not in its absolute value, all three absorption profiles in Figure 2a are shown on a relative scale. Each spectrum shows four well-developed satellite bands. In the far line-wing region there is a group of three distinct satellite bands ("a", "b", "c"), and in the near-wing a weak structure (labeled "d") is discernible. The satellite bands are resting on a background caused by the long-wavelength tail of the B $^1\Pi_u$– X $^1\Sigma_g^+$ molecular band [17] and possibly by the short-wavelength tail of the A $^1\Sigma_u^+$ – X $^1\Sigma_g^+$ molecular band [34], as discussed below. However, the discrete molecular spectral lines belonging to the B-X and, possibly, to the A-X molecular bands, cannot be resolved using our present monochromator.

Three outermost satellites, "a" at 817 nm , "b" at 827 nm, and "c" at 835 nm, have the same characteristic shape with an exponential falloff beyond the satellite peak (towards shorter wavelengths). This strongly suggests that each of these bands is caused by a local maximum in the corresponding difference-potential curve [23,9]. Careful inspection of the "d" satellite band region (from 838 nm to

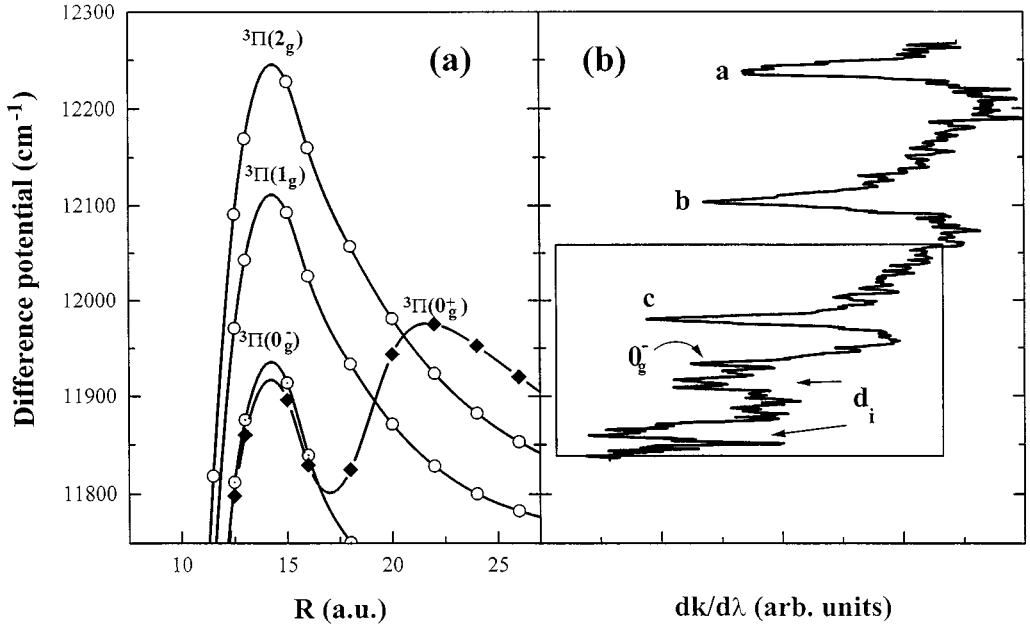

Fig. 3. (a) The difference-potential curves [32] relevant to the explanation of the observed satellite bands. (b) The first derivative of the absorption line-wing shape labeled "1" (from Fig. 2). Note the one-to-one correspondence between the positions of the classical satellite band peaks "a", "b", and "c", and the maxima in the relevant difference-potential energy curves.

842 nm) shows that it is more pronounced at higher temperature. Unfortunately, this satellite band is sitting on a very strong and steeply rising resonance line wing. As a consequence, such a weak and diffuse structure is hardly discernible from the strong line wing even at the highest cell temperature. In order to obtain a better insight into the details of the spectrum, and to make a more sensitive comparison with the calculated spectrum, we performed a numerical differentiation of each experimental absorption spectrum. The corresponding numerically differentiated profiles are shown in Figure 2b. The differentiation enhances the features of the absorption profile, revealing the rainbow satellite as a sharp peak [25], giving *exactly* the position of the local extremum in the difference-potential-energy curve (see Fig. 3 and Tab. 1). The molecular background mentioned before now appears as a reproducible spiky structure extending over the observed satellite region. This background structure is visible only in the presentation $\mathrm{d}k/\mathrm{d}\lambda$ *vs.* $\Delta\lambda$; in the presentation k *vs.* $\Delta\lambda$ these intensity variations are by far too small to be visible. The contrast between the satellite peaks and the molecular background changes with temperature. At higher T_c the background structure is much weaker compared with the peak satellite intensity. This background cannot be a simple residual noise because (a) each trace represents a statistical average of five exactly overlapped experimental scans and (b) the majority of the spiky oscillations are reproducibly present in all three spectra (labeled 1, 2, and 3). This is a strong indication that they could be caused by the residual intensity of the discrete molecular lines belonging to the long-wavelength tail of the Cs_2 B-X band, and possibly to the short-wavelength tail of the Cs_2 A-X band. The spectrum recorded at the highest T_b and T_c (labeled "1") is least influenced by these background oscillations, and we used that spectrum for further analysis and comparison with our satellite-shape calculations.

3.2 Interpretation

In order to get satisfactory agreement between the measured and calculated shape and the position of the satellite band, it is necessary to have a reliable set of corresponding potential-energy curves and transition-dipole moments generating the observed spectrum. In this work we used the Cs_2 potential-energy curves calculated by Spiess and Meyer [31,32] to obtain the corresponding difference-potential curves and the transition-dipole moment needed for the simulation of the measured spectrum.

Figure 3 shows a comparison of the relevant difference-potential curves and the spectrum labeled "1" in Figure 2b (see also Tab. 1). There is an unambiguous one-to-one correspondence between the most pronounced satellite bands "a", "b" and "c" at 817 nm, 827 nm, and 835 nm, respectively, and the local extrema in the difference potentials 2_g, 1_g (both at an interatomic distance of about 14 a.u.), and 0_g^+ (at an interatomic distance of about 22 a.u.) emerging from the $6\,^2\mathrm{P}_{3/2} + 6\,^2\mathrm{S}_{1/2}$ asymptote [9]. The shape and position of these three isolated satellites can be reproduced using the data on the related difference-potential curves and the appropriate theoretical approach (see, *e.g.*, [24] and [25]). On the other hand, the origin of the merged satellite bands at 838-842 nm is not so obvious. The peak labeled "0_g^-" may be definitely associated with the local maximum of the $1\,^3\Pi_g(0_g^-) - a\,^3\Sigma_u^+(1_u)$ difference-potential curve at about 14 a.u. (it is interesting to note that this potential-energy curve gives rise to the pure long-range cesium molecule in the far long-range region, as discussed in [35]). In addition, the second local maximum in the $1\,^3\Pi_g(0_g^+) - a\,^3\Sigma_u^+(1_u)$ difference-potential curve at about 14 a.u. contributes to this region, too. However, the bands labeled "d_i" cannot be related to any local extremum in any of the potentials. We will show that their appearance and shape are related to the interference

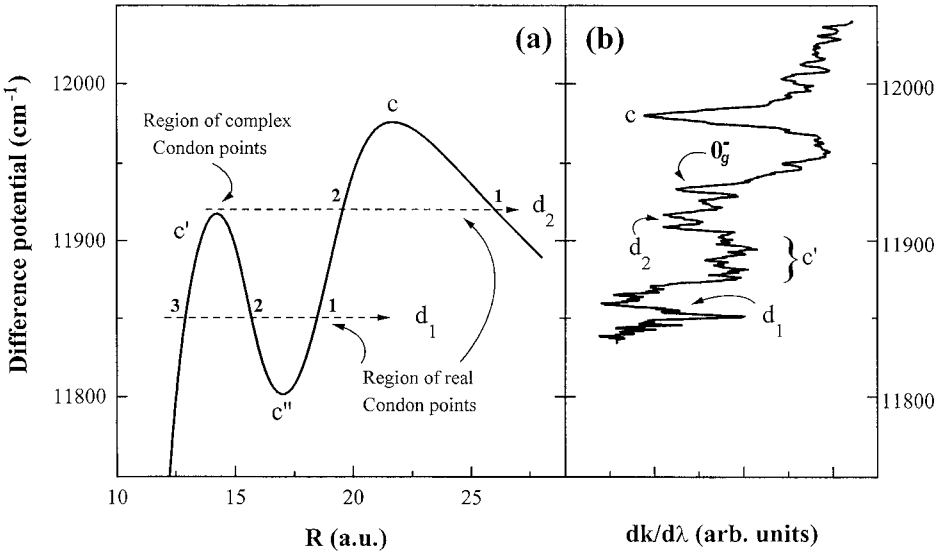

Fig. 4. The comparison of the $a\,^3\Sigma_u^+(1_u) \rightarrow 1\,^3\Pi_g(0_g^+)$ difference-potential curve, (a), and the first derivative of the absorption line-wing, (b), in the region from 11825 cm^{-1} to 12025 cm^{-1}.

effect occurring between pairs of Condon points belonging to the $1\,^3\Pi_g(0_g^+) - a\,^3\Sigma_u^+(1_u)$ difference-potential curve.

In order to make the identification of these satellite bands more transparent and to enable one to make a clearer comparison between the measured and the calculated satellite band shape, in Figure 4 we show only the difference-potential curve $1\,^3\Pi_g(0_g^+) - a\,^3\Sigma_u^+(1_u)$ and the enlarged part of Figure 3b. The difference-potential curve is smoothly continued beyond 27 a.u. towards $R \rightarrow \infty$ using the correct asymptotic dependence (the dipole-dipole resonant and van der Waals interactions). This potential curve is further used in the calculations of the power spectrum (the line wing and the satellite shape) belonging to this potential.

4 Theoretical treatment

Following the approach described in detail by Holstein [36] and Sobel'man [21], the time-dependent phase of a classical oscillator can be expressed as

$$f(E,b,\omega,t) = \frac{1}{\hbar}\int_{-\infty}^{t} \left(\Delta V_{f,i}\left(R\left(E,b,t'\right)\right) - \hbar\omega\right) \mathrm{d}t'. \quad (3)$$

Here ω is the oscillator frequency in the absence of collisions, $\Delta V_{f,i}$ is the corresponding difference-potential curve, R is the interatomic distance, E is the kinetic energy of the colliding particles, and b is the impact parameter. In this description the atomic oscillator is assumed to be only adiabatically perturbed during the collision event.

The power spectrum of a classical atomic oscillator is given by

$$C(E,b,\omega) = \frac{1}{\sqrt{2\pi\tau}}\int_{-\frac{\tau}{2}}^{\frac{\tau}{2}} \mathrm{e}^{if(E,b,\omega,t)} D(t)\mathrm{d}t, \quad (4)$$

where C is the Fourier transform of the phase of the classical oscillator given by equation (3). D(t) is the corresponding electronic transition dipole moment. The reduced absorption coefficient is given by

$$k(T,\omega) = \frac{8\pi\omega}{3c}\left\langle \left|C(E,b,\omega)\right|^2 \right\rangle_{E,b}, \quad (5)$$

where the brackets $\langle ... \rangle_{E,b}$ denote the averaging over collision energies and the summation over impact parameters at a temperature T. In order to simplify the calculation of the reduced absorption coefficient and still secure a qualitatively correct spectrum, we used the constant radial-velocity approximation

$$v_{\mathrm{r}}(E,b) = \left[\frac{2}{m}\left(E - V\left(R_0\right) - \frac{Eb^2}{R_0^2}\right)\right]^2, \quad (6)$$

where V is the initial (ground-state) electronic potential and R_0 is a fixed internuclear distance from the range of internuclear separations where extrema in the difference-potential curve appear.

Using the constant radial-velocity approximation, the classical motion of colliding particles in the vicinity of R_0 can be described by the expression

$$R(E,b,t) = R_0 + v_{\mathrm{r}}(E,b)(t - t_0), \quad (7)$$

where $R_0 = R(t_0)$.

The summation over the impact parameter b and the collision energy E in equation (5) can be reduced to the

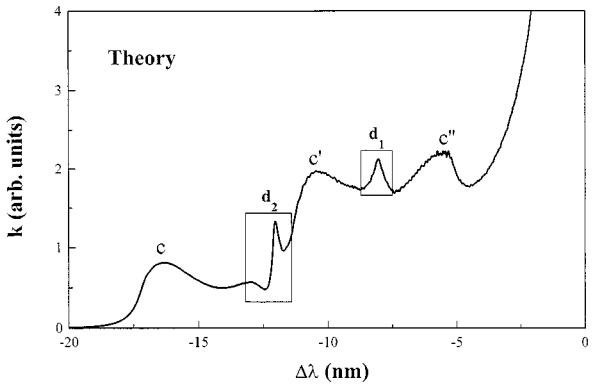

Fig. 5. The contribution from the $a\,^3\Sigma_u^+(1_u) \rightarrow 1\,^3\Pi_g(0_g^+)$ difference-potential curve to the total absorption coefficient in the blue wing of the Cs D_2 resonance line.

single integration after integration by parts [37]:

$$\left\langle |C(E,b,\omega)|^2 \right\rangle_{Av} = 2\left(\frac{2\pi}{m}\right)^{\frac{1}{2}} (KT)^{\frac{3}{2}} R_0^2\, \mathrm{e}^{-\frac{V_i(R_0)}{KT}} \times \int_0^\infty \mathrm{e}^{-\frac{E}{KT}} |C(E,b=0,\omega)|^2\, \mathrm{d}E. \quad (8)$$

The factor $|C(E,b=0,\omega)|^2$ represents the power spectrum for the impact parameter $b = 0$, which is the consequence of the constant radial-velocity approximation. Figure 5 shows the results of this calculation, the spectrum generated solely by the $1\,^3\Pi_g(0_g^+) - a\,^3\Sigma_u^+(1_u)$ difference-potential, at a temperature corresponding to our experimental conditions. The theoretical spectrum in Figure 5 shows that the calculation predicts three kinds of satellite bands. First, the Fourier transform approach generates a correct, well-known shape of the ("rainbow") satellite bands caused by local extrema in the difference-potential curve. The features labeled with c, c″, and c′ correspond to the local extrema in the $1\,^3\Pi_g(0_g^+) - a\,^3\Sigma_u^+(1_u)$ difference-potential curve at about 22 a.u., 17 a.u., and 14 a.u., respectively. As noted before, the shape of these satellites can be alternatively calculated using the standard approach to the calculation of the one-perturber satellite band [24]. However, in this case, each of these bands must be calculated separately, using the points around each local extremum in the $1\,^3\Pi_g(0_g^+) - a\,^3\Sigma_u^+(1_u)$ difference-potential-energy curve. On the contrary, the use of the Fourier transform technique has a very important advantage that it generates the complete line-wing shape simultaneously, taking into account all points of the difference-potential curve involved. The second kind of satellite band, labeled d_1, is an example of a nonclassical satellite caused by an interplay of three Condon points (see Fig. 4). The third type of satellite band, labeled d_2, is also a nonclassical satellite band caused by a part of the difference-potential curve dominated by four (two real and two complex) stationary points.

In Figure 6 we show the *derivatives* of the measured (Figs. 2b and 4b) and the calculated (Fig. 5)

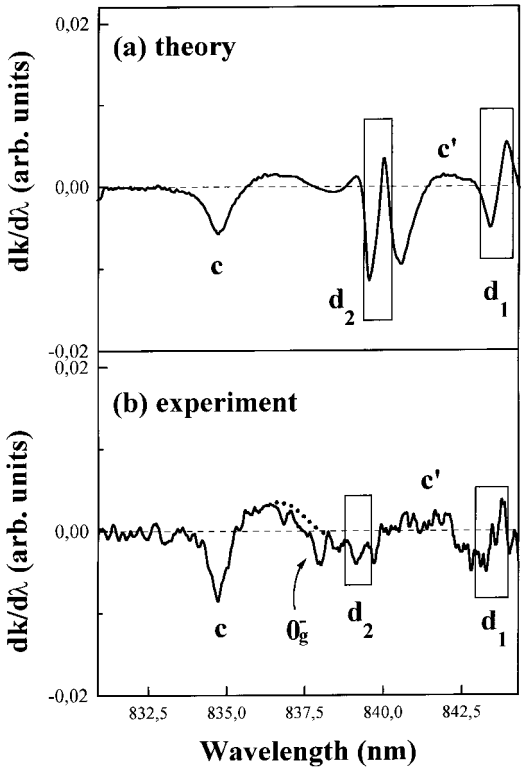

Fig. 6. The comparison of the calculated (a) and measured (b) first derivatives of the satellite band shapes caused solely by the $a\,^3\Sigma_u^+(1_u) \rightarrow 1\,^3\Pi_g(0_g^+)$ difference-potential curve. The dotted line at 837.5 nm denotes the assumed band shape generated only by this difference-potential curve after subtraction of the 0_g^- satellite band.

satellite shapes. Comparing these spectra, we have to take into account that the experimental spectrum originates from the superposition of several transitions $(1\,^3\Pi_g(2_g, 1_g, 0_g^+, 0_g^-) \leftarrow a\,^3\Sigma_u^+(1_u, 0_u^-)$, see Fig. 3a), including the contributions from the long-wavelength tail of the cesium dimer B-X band, and possibly from the short-wavelength tail of the Cs_2 A-X band. All these contributions (except $1\,^3\Pi_g(0_g^-) \leftarrow a\,^3\Sigma_u^+(1_u, 0_u^-)$) are monotonic in the spectral region between 11850 and 12000 cm^{-1}, and can be subtracted simply as a straight line in the $\mathrm{d}k/\mathrm{d}\lambda$ *vs.* $\Delta\lambda$ presentation. The peak corresponding to the satellite caused by the $1\,^3\Pi_g(0_g^-) - a\,^3\Sigma_u^+(1_u)$ difference-potential curve is clearly marked, and the approximate background belonging solely to the $1\,^3\Pi_g(0_g^+) - a\,^3\Sigma_u^+(1_u)$ difference-potential curve is indicated by a dotted line. Consequently, the experimental absorption profile given in Figure 6b is caused only by the $1\,^3\Pi_g(0_g^+) - a\,^3\Sigma_u^+(1_u)$ difference-potential curve.

5 Discussion

The shape of the investigated satellite bands is decisively dependent on the shape of the complete difference-potential curve, and only partially on the corresponding transition dipole moment. The case of rainbow-satellite bands has often been studied during the last two decades

(see, *e.g.*, the recent review [29]), and will not be particularly discussed here. However, to the best of our knowledge, the cusp-shaped satellite bands (spectral features labeled d_1 and d_2 in our spectra) have been observed and explained here for the first time. Their appearance and shape can be explained using catastrophe theory [38,39]. The presented observation of the far-wing cesium satellites is a rare example of an optical transition where four closely related Condon points determine the shape of the corresponding spectrum.

Inspection of the spectra in Figures 5 and 6 shows that the calculation predicts and the experiment reveals three kinds of satellite bands. The first kind are the so-called rainbow satellite bands labeled with c, c′, and c″. They can be understood in the framework of the uniform Airy theory of satellite bands [29]. These spectral features are dominated by the influence of transitions generated by two close stationary points in the vicinity of an extremum in the difference-potential curve. On the other hand, the case where two stationary points dominate the transition has been known for a long time in the theory of catastrophes as the fold catastrophe case [39], and the related Fourier integral used here for the calculation of the satellite shape (Eq. (4)) belongs to the class of canonical integrals investigated within that theory. In this case, the canonical integral can be approximated by a linear combination of Airy functions [38,40], and the catastrophe manifold can be uniformly mapped to a parabola. Consequently, the shape of any rainbow one-perturber satellite can be alternatively explained and calculated using the results of the fold catastrophe theory.

The second spectral feature labeled d_1 is the first example of a nonclassical satellite band caused by an interplay of three Condon points in the region about 11850 cm^{-1}. The three Condon points, labeled 1, 2, and 3, interfere pairwise, so that pairs of points (1, 2) and (2, 3) experience only destructive interference with a negligible spectral contribution [41]. However, two outer Condon points (1 and 3) interfere constructively, which results in a sharp cusp-shaped satellite labeled d_1. The cusp position in the spectrum corresponds to the range of transition energies where the difference in phase of the atomic oscillator at two outer Condon points tends to zero:

$$f(R_1) - f(R_3) \approx 0. \tag{9}$$

This spectral feature, caused by three real stationary points, can be linked to the catastrophe of higher order (cusp catastrophe, Ref. [42]). The corresponding catastrophe manifold can be uniformly mapped to a cubic parabola and, in this case, the canonical integral corresponds to the Pearcy integral [42]. The shape of this satellite band can be explained *only* using the results of the cusp catastrophe theory. The prediction of such a type of satellite rainbow was given by Beuc *et al.* [43].

The third spectral feature, labeled d_2, is perhaps the most intriguing one. It is an additional example of a nonclassical satellite band caused by a part of the difference-potential curve in the vicinity of 11925 cm^{-1}, dominated by four stationary points – two real and two complex. This region of the $1\,^3\Pi_g(0_g^+) - a\,^3\Sigma_u^+(1_u)$ difference-potential curve belongs to the catastrophe manifold that can be uniformly mapped to a biquadratic function. The spectral position of the cusp labeled d_2 corresponds to the range of transition energies (see Fig. 4) where the phase difference between the real Condon point R_{r1} and the pair of complex Condon points (R_{c1}, R_{c2}) tends to zero:

$$f(R_{r1}) - f(R_{c1;c2}) \approx 0. \tag{10}$$

As in the preceding case, the shape of such a satellite can be explained *only* using the results of the catastrophe of the next (higher) order (swallow-tail catastrophe [39]).

Taking into account that the comparison of the derivatives of the absorption coefficient (Fig. 6) is very sensitive to the shape of satellite bands, the general resemblance of the derivatives of the measured and the calculated satellites is satisfactory. The calculated spectrum reveals practically all features of the measured satellite bands: the rainbow satellite band c at 835 nm, the second rainbow satellite band c′ at about 842 nm, the first type of the cusp-satellite d_1 at about 843 nm, and the second type of the cusp-satellite d_2 at about 838 nm. The swing of the $dk/d\lambda$ around the zero-line in the range 836 nm and 842 nm is similar in both the calculated and the experimental spectrum. The position and shape of the measured and the calculated rainbow satellites c and c′, and the cusp-satellite d_1 almost coincide. However, the measured higher-order cusp-satellite d_2, compared with the calculated one, shows the most significant difference: the intensity of the calculated satellite is stronger than the intensity of the measured one. The existing discrepancy can, perhaps, be partially attributed to the discrepancy of the finest details of the calculated and the real difference-potential-energy curve. In addition, a more elaborate theoretical treatment might reveal the importance of the free-bound $a\,^3\Sigma_u^+(1_u) \rightarrow 1\,^3\Pi_g(0_g^+)$ transitions which have not been taken into account in the present analysis. The existence of bound states in the $^3\Pi_g(0_g^+(^2P_{3/2}))$ potential-energy curve of alkali dimers is discussed in [44], especially for K_2 and Rb_2 molecules. This can also lead to the smearing of the calculated satellite band shape.

In principle, the satellite bands can experience smearing also as a consequence of nonadiabaticity of the potential-energy curves involved in the transition. The difference-potential curve $a\,^3\Sigma_u^+(1_u) \rightarrow 1\,^3\Pi_g(0_g^+)$ (Fig. 4) has this unique double-minimum shape because of the strong avoided crossing of the $0_g^+(^1\Sigma_g^+(^2P_{1/2}))$ and the $0_g^+(^3\Pi_g(^2P_{3/2}))$ potential-energy curves. In principle, there is a certain amount of probability that during the collision event the atoms may change the current state and jump from one 0_g^+ adiabatic potential curve to another one. This can also lead to the smearing of the measured satellite band shape. The measure of the validity of the adiabatic approach is the Massey parameter [45]: in the range of internuclear separations where the Massey parameter is large ($\gg$1) the system is well described by the adiabatic potential curves. This criterion is generally satisfied for heavier alkali molecules and specifically in the present particular case of Cs_2 molecule. As the cause

of additional smearing of the satellite bands, the nonadiabatic effects (the nonradiative transitions in the region of avoided crossing of the $0_g^+(^1\Sigma_g^+(^2P_{1/2}))$ and the $0_g^+(^3\Pi_g(^2P_{3/2}))$ potential-energy curves), can be ruled out in the Cs_2 case.

6 Conclusion

We have performed absorption measurements of the far-wing satellites of the cesium D_2 resonance line and compared the results with the satellite band shape calculated using the Fourier transform technique and a set of high-quality Cs_2 potential-energy curves. The analysis of the experimental and theoretical satellite shapes reveals the presence of the rainbow and nonclassical cusp-shaped satellite bands. We have provided the assignment and explanation of the rainbow and cusp-shaped satellite bands. Although the origin of rainbow satellite bands was for the first time discussed almost twenty years ago, cusp-shaped satellite bands have been observed and explained here for the first time. Comparison of the experimental and the calculated satellite shapes shows good agreement, and owing to the high quality of the available set of the potential-energy curves, even fine details of the satellite bands can be reproduced. The nonclassical cusp-shaped satellites are discussed in terms of catastrophe theories. We have shown that the appearance and the shape of these satellite bands are a consequence of catastrophes of higher order (cusp and swallow-tail catastrophe).

We are grateful to Prof. W. Meyer for allowing us the use of his calculated cesium potential-energy curves prior to publication of his data. This research was supported by the grant JF107/NIST/Veža of the USA-Croatia Joint Fund for Cooperation in Science and Technology and by the Ministry of Science and Technology of the Republic of Croatia.

References

1. C. Amiot, C. Crépin, J. Vergès, J. Mol. Spectrosc. **107**, 28 (1984).
2. H. Kato, T. Kobayashi, M. Chosa, T. Nakahari, T. Iida, S. Kasahara, M. Baba , J. Chem. Phys. **94**, 2600 (1991).
3. T. Kobayashi, T. Usui, T. Kumauchi, M. Baba, K. Ishikawa, H. Katô, J. Chem. Phys. **98**, 2670 (1993).
4. M. Raab, G. Höning, W. Demtröder, C.R. Vidal, J. Chem. Phys. **76**, 4370 (1982).
5. U. Diemer, R. Duschowicz, M. Ertel, E. Mehdizadeh, W. Demtröder, Chem. Phys. Lett. **164**, 419 (1989).
6. J. Verges, C. Amiot, J. Mol. Spectrosc. **126**, 393 (1987).
7. H. Wieckenmeier, U. Diemer, M. Wahl, M. Raab, W. Demtröder, W. Müller, J. Chem. Phys. **82**, 5354 (1985).
8. C. Amiot, C. Crépin, J. Vergès, Chem. Phys. Lett. **106**, 162 (1984).
9. G. Pichler, M. Movre, D. Veža, K. Niemax, in *Proc. 33rd Symp. on Molec. Spectroscopy* (Columbus, Ohio, June 12-16) TF11 (1978).
10. J. Huennekens, Z. Wu, T.G. Walker, Phys. Rev. A **31**, 196 (1985).
11. G.V. Pitatelev, V.I. Lukashenko, Opt. Commun. **55**, 110 (1985).
12. G. Pichler, S. Milošević, D. Veža, R. Beuc, J. Phys. B: At. Mol. Phys. **16**, 4619 (1983) and references therein.
13. U. Diemer, J. Gress, W. Demtröder, Chem. Phys. Lett. **178**, 330 (1991).
14. G.L. Bhale, A. Sasso, W. Demtröder, Chem. Phys. Lett. **188**, 376 (1992).
15. B. Kim, K. Yoshihara, Chem. Phys. Lett. **204**, 407 (1993).
16. F.W. Loomis, P. Kusch, Phys. Rev. **46**, 292 (1934).
17. P. Kusch, M.M. Hessel, J. Mol. Spectrosc. **32**, 181 (1969).
18. K. Niemax, G. Pichler, J. Phys. B: At. Mol. Phys. **7**, 2355 (1974).
19. M. Movre, G. Pichler, J. Phys. B: At. Mol. Phys. **10**, 2631 (1977).
20. M. Movre, G. Pichler, J. Phys. B: At. Mol. Phys. **13**, 697 (1980).
21. I.I. Sobelman, in *Introduction to the Theory of Atomic Spectra* (Pergamon, Oxford, 1973).
22. J. Cooper, in *Comments on the theory of satellite bands*, JILA Report No 111 (1973).
23. J. Szudy, W.E. Baylis, J. Quant. Spectrosc. Radiat. Trans. **15**, 641 (1975).
24. D. Veža, M. Movre, G. Pichler, J. Phys. B: At. Mol. Phys. **13**, 3605 (1980).
25. R. Beuc, V. Horvatić, J. Phys. B: At. Mol. Opt. Phys. **25**, 1497 (1994).
26. R. Beuc, S. Milošević, M. Movre, G. Pichler, D. Veža, Fizika **14**, 345 (1982).
27. R. Côte, A. Dalgarno, Y. Sun, R.G. Hulet, Phys. Rev. Lett. **74**, 3581 (1995).
28. M.H. Anderson, J.R. Ensher, M.R. Matthew, C.E. Wieman, E.A. Cornell, Science **269**, 198 (1995).
29. J. Szudy, W.E. Baylis, Physics Reports **266,** 128 (1996).
30. H. Pauly, in *Atom-Molecule Collision Theory*, edited by R.B. Bernstein (Plenum Press 1979).
31. W. Meyer, N. Spiess, private communication.
32. N. Spiess, Ph.D. Thesis, University of Kaiserslautern, (1989) (unpublished). Note: Following a comment in this reference to obtain a correct asymptotic behavior, all potential-energy curves belonging to the $6\,^2S_{1/2} + 6\,^2P_{3/2}$ atomic asymptote must be shifted by $+14$ cm^{-1}.
33. J.B. Taylor, I. Langmuir, Phys. Rev. **15**, 753 (1937).
34. R.P. Benedict, D.L. Drummond, L.A. Schlie, J. Chem. Phys. **66**, 4600 (1977).
35. W.C. Stwalley, Y.-H. Uang, G. Pichler, Phys. Rev. Lett. **41,** 1164 (1978).
36. T. Holstein, in *Pressure Broadening of Spectral Lines* (University of Pittsburgh, internal report, 1953).
37. K.M. Sando, J.C. Wormhoudt, Phys. Rev. A **7**, 1889 (1973).
38. J.N.L. Connor, R.A. Marcus, J. Chem. Phys. **55**, 5636 (1971).
39. J.N.L. Connor, Mol. Phys. **31**, 33 (1976).
40. K.M. Sando, Phys. Rev. A **7**, 1889 (1973).
41. R. Beuc, Ph. D. Thesis, University of Zagreb, 1993 (unpublished).
42. J.N.L. Connor, D. Farrelly, J. Chem. Phys. **75**, 2831 (1981).
43. R. Beuc, M. Movre, in *Proc. 9th International Conference on Spectral Line Shapes* (Torun, Poland, July 25-29) D3 (1988).
44. O. Dulieu, R. Kosloff, F. Masnou-Seeuws, G. Pichler (to be published).
45. N.F. Mott, H.S.W. Massey, in *The Theory of Atomic Collisions* (Oxford, 1952).